J. Fluid Mech. (1972), *vol.* 56, *part* 1, *pp.* 19–47
Printed in Great Britain

The boundary layer in a shock tube

By J. D. A. WALKER
Department of Mathematics, University College London
AND S. C. R. DENNIS
Department of Applied Mathematics, University of Western Ontario

(Received 3 May 1972)

The boundary layer that forms on the walls of a shock tube, after the diaphragm which initially separates two gases at different pressures is burst, is investigated. Both the driver and driven gases are assumed to have the same thermal properties and the shock tube wall is maintained at constant temperature. Crocco variables are used and a method is presented for solving the compressible boundary-layer equations within the tube in similarity variables. Three cases, corresponding to different initial pressure ratios of the driver and driven gases, are calculated which are representative of weak and medium-strength shock and expansion waves.

1. Introduction

1.1. *General description*

Consider a thin diaphragm at $x = 0$ in an infinitely long cylindrical shock tube, separating two gases at different pressures. Suppose that the gas to the left of the diaphragm has a higher pressure p_l than that to the right (p_r), so that the pressure ratio $P_R = p_l/p_r > 1$. At $t = 0$ the diaphragm is suddenly burst. Ideally this causes a shock wave to advance into the undisturbed fluid to the right at constant speed U_s, which is subsequently followed by a contact surface moving with constant speed U_0. The fluid between the contact surface and the shock was originally in $x > 0$ and has acquired a velocity U_0 abruptly, upon passing through the shock. Across the contact surface the fluid temperature and density are discontinuous while the pressure and velocity must be continuous. The undisturbed fluid to the left of the diaphragm is sucked through an expansion wave advancing to the left, and achieves a speed U_0 at the end of the wave.

The inviscid unsteady flow that develops in the shock tube after the diaphragm is burst was given by Riemann in 1860 and has been described by Shapiro (1960, p. 1418). The objective of the present paper is to study the laminar boundary layer that forms on the walls of the shock tube and extends from the leading edge of the expansion wave to the foot of the shock. The flow may be divided into four distinct regions (shown in figure 1, at time t): (i) that in the expansion fan, E; (ii) that between the end of the fan and the burst diaphragm, L; (iii) the interaction region between the diaphragm and the contact surface, I; (iv) that between the contact surface and the shock, M.

It should be noted that, if the initial pressure difference P_R is large enough, the

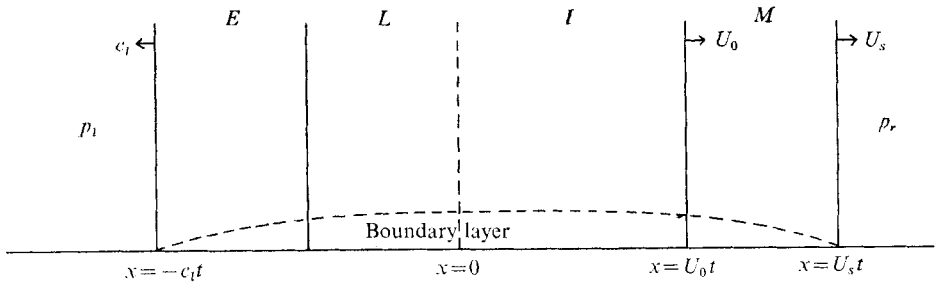

FIGURE 1. Shock tube flow (c_l is the sound speed of the undisturbed gas).

fan will extend into the I region and there will be no L region. In the present paper, this case will not be considered and only cases of medium-strength waves, where the region L is of non-zero thickness will be treated.

Various authors have considered this problem. Mirels (1955) obtained a solution for the boundary layer behind a shock wave advancing over an infinite flat plate. This solution is a valid one for the present problem in the M region. Subsequently, Mirels (1956) extended his previous work to the case of an infinitely thin expansion wave advancing along an infinite flat plate. If the E region is very thin (weak waves), this solution will approximate the flow in the L region. Cohen (1957) obtained a solution in the fan, by expanding the flow variables in a power series in a variable which measured distance from the front of the fan. His solution is valid in the E region downstream of the leading edge of the fan to approximately $x \approx -0{\cdot}7c_lt$, where c_l is the sound speed of the undisturbed gas. In theory, Cohen's solution could be extended to $x = 0$ by taking more terms in the series and an attempt was made by Becker (1962) to extend the solution to $x = 0$ by a continuation procedure.

Thus the solution in the M region is well known while the solution in the E and L regions have been given approximate treatment. The solution in the I region is a mathematically more difficult problem and a recent paper by Ban & Kuerti (1969), who treated the case of weak waves approximately, is the only solution available in this region.

This problem is intimately connected with two other problems. Stewartson (1951) considered the problem of a semi-infinite flat plate impulsively started from rest at $t = 0$, to achieve a velocity U_0. Let x measure the distance from the leading edge of the plate and $\tau = U_0t/x$. For small τ, the solution is that given by Rayleigh (1911) since for any x the boundary layer is not aware of the presence of the leading edge. At $\tau = 1$, Stewartson (1951) found an essential singularity such that the solution for $\tau < 1$ was not an analytic continuation of the solution for $\tau > 1$, although all derivatives with respect to τ are continuous there. Physically, for any x, $\tau = 1$ corresponds to the first time the flow is aware of the leading edge. Finally as $\tau \to \infty$, the solution must approach that given by Blasius (1908). The problem of how to describe the transient motion between the Rayleigh and Blasius solution was eventually solved numerically by Hall (1969) and later by Dennis (1972). The major difficulty with solving this problem is that if the equations of motion are written in similarity variables $\eta = y\,(U_0/\nu x)^{\frac{1}{2}}$,

$\tau = U_0 t/x$ (y measuring normal distance from the plate), thus reducing the number of independent variables from three to two, the equations are singular-parabolic in the region $\tau > 1$. The equations are of first order in τ and second order in η; the coefficient of the τ derivative is $1 - u\tau/U_0$ and for $\tau > 1$, it will vanish and change sign somewhere in the boundary layer. Effectively this means that standard numerical marching techniques in this region will fail. Hall (1969) overcame the problem by solving the equations in the x, y, t space between the planes $x = 1$ and $x = 2$; Dennis (1972), by using the Rayleigh (1911) solution as a boundary condition at $\tau = 1$ and the Blasius (1908) solution for a large value of τ, used a special numerical procedure to solve the problem in similarity variables as a boundary-value problem. The question of how the variable x enters the solution at $\tau = 1+$ has only recently been clarified by Stewartson (1972).

Lam & Crocco (1958) considered the problem of a shock advancing over a semi-infinite flat plate (which is identical with Stewartson's for very weak shocks) and found that two boundary conditions must be enforced at $x = 0$ and $x = U_0 t$, where x measures distance from the leading edge and U_0 is the speed of the fluid in the free stream following the shock. Using the boundary-layer equations written in Crocco variables, they found that the similarity equations are singular-parabolic between $x = 0$ and a Stewartson singularity at $x = U_0 t$. Physically, this is the region where there is an interaction with the boundary layer created by the passage of the shock and the downstream influence of the leading edge.

Ban & Kuerti (1969) first considered the flow in the interaction region of a shock tube but considered only the case of weak shock and expansion waves. Using a linearization scheme, they produced a solution for an initial pressure difference of $P_R = 1{\cdot}35$. In the shock tube problem there is a Stewartson singularity at the contact surface $x = U_0 t$ and the equations are singular-parabolic between the diaphragm ($x = 0$) and $x = U_0 t$. In the present paper the work of Ban & Kuerti (1969) is extended to consider (*a*) the case of medium-strength shock and expansion waves, where medium implies that the expansion wave does not extend into the interaction region, (*b*) the effect of finite thickness expansion waves and (*c*) the full nonlinear equations. Three cases corresponding to three different initial pressure ratios $P_R = 2$, 6 and 10 for an air–air shock tube with Prandtl number $\sigma = 0{\cdot}73$ were considered. The problem is formulated in Crocco variables and then in similarity variables, thus reducing the number of independent variables from three to two. The solutions were integrated numerically from the leading edge of the fan, through the fan and then through the L region to the diaphragm. These solutions were used as boundary conditions at $x = 0$ for the interaction region while the solutions in the M region were used as boundary conditions at $x = U_0 t$. The problem was then solved numerically in the interaction zone using the method of Dennis (1972).

While no experimental data in the boundary layer seems to be available for the E, L and I regions, good agreement is obtained with Cohen's (1957) and Ban & Kuerti's (1969) theoretical results.

1.2. *Basic equations*

The general problem of flow in a shock tube is an extremely complicated one and to make progress it is necessary in the present paper to make certain simplifying assumptions at the outset. Turbulence, chemical reactions and diaphragm-opening effects all complicate the picture and these phenomena will be excluded. Further, it is assumed that (*a*) the two-dimensional compressible laminar boundary-layer equations describe the flow, (*b*) the contact surface, shock wave and boundaries of the expansion fan remain planar, (*c*) the wall temperature T_w of the tube is constant and is equal to the temperature of the undisturbed gas on either side of the diaphragm, (*d*) the driven and driver gases have the same constant Prandtl number σ and specific heat ratio γ, (*e*) the speeds U_0, U_s and c_l are constant as in Riemann's solution and (*f*) the gases obey the perfect gas law $p = \rho RT$. Finally, for convenience the constant parameters $A = U_s/U_0$ and $B = c_l/U_0$ are defined.

A particularly convenient formulation for compressible flow problems, in which separation does not occur, is to introduce Crocco variables. The shearing stress $\tau(x, u, t) = \mu\, \partial u/\partial y$ is taken as the dependent variable. Here y measures distance normal to the wall, u is the fluid velocity in the direction of x increasing and μ is the absolute viscosity. In terms of the independent variables (x, u, t), the two-dimensional compressible boundary-layer equations for τ and the specific enthalpy $h(x, u, t)$ are

$$\frac{\partial^2 \tau}{\partial u^2} + \frac{\partial}{\partial t}\left(\frac{\rho\mu}{\tau}\right) + u\frac{\partial}{\partial x}\left(\frac{\rho\mu}{\tau}\right) - \frac{\partial}{\partial u}\left(\frac{\mu}{\tau}\right)\frac{\partial p}{\partial x} = 0, \tag{1}$$

$$\rho\mu\left\{\frac{\partial h}{\partial t} + u\frac{\partial h}{\partial x}\right\} + \left\{\frac{1}{2}\left(1 - \frac{1}{\sigma}\right)\frac{\partial}{\partial u}(\tau^2) - \mu\frac{\partial p}{\partial x}\right\}\frac{\partial h}{\partial u} = \mu\frac{\partial p}{\partial t} + \mu u\frac{\partial p}{\partial x} + \tau^2\left\{1 + \frac{1}{\sigma}\frac{\partial^2 h}{\partial u^2}\right\}, \tag{2}$$

where p is the fluid pressure and ρ is the density. The boundary conditions are

$$\tau\, \partial\tau/\partial u = \mu\, \partial p/\partial x \quad \text{at} \quad u = 0, \qquad \tau = 0 \quad \text{at} \quad u = U_1(x, t), \tag{3}$$

and

$$h = \text{constant} = h_w \quad \text{at} \quad u = 0, \qquad h = h_1(x, t) \quad \text{at} \quad u = U_1(x, t). \tag{4}$$

Here $U_1(x, t)$ and $h_1(x, t)$ are the speed and enthalpy of the inviscid flow respectively. The number of independent variables may be reduced from three to two by introducing similarity variables. This is now done in the various regions of the flow and the solution in each considered separately.

2. The expansion fan

2.1. *Governing equations*

New dimensionless independent and dependent variables are introduced in the region E:

$$\left.\begin{aligned} \xi = 1 + x/c_l t, \quad \eta = u/c_l, \quad \Omega = \rho_l c_l^2 t/\mu_l, \\ \tau = \rho_l c_l^2 \Phi \Omega^{-\frac{1}{2}}, \quad H = (h - h_w)/h_w, \quad P = p/\rho_l c_l^2. \end{aligned}\right\} \tag{5}$$

Here the subscript l is used to indicate quantities evaluated in the undisturbed high pressure gas to the left of E. The enthalpy in this region $h_l = h_w$, the wall

enthalpy. The fluid quantities within the inviscid free stream in the fan are well known and are reproduced below. They are denoted by a subscript 1 and using a tilde to indicate a non-dimensional quantity,

$$\left.\begin{aligned} \tilde{U}_1 &= \frac{U_1}{c_l} = \frac{2\xi}{\gamma+1}, \quad \tilde{c}_1 = \frac{c_1}{c_l} = 1-\frac{\gamma-1}{\gamma+1}\xi, \\ \tilde{h}_1 &= h_1/h_w = \tilde{c}_1^2, \quad \tilde{p}_1 = p_1/p_l = \tilde{c}_1^{2\gamma/(\gamma-1)}. \end{aligned}\right\} \tag{6}$$

In view of the sole dependence of the free-stream quantities on the conical variable ξ, it is natural to seek solutions containing conical similarity. A self-similar time dependence is anticipated by assuming $\Phi = \Phi(\xi, \eta)$ and $H = H(\xi, \eta)$.

One further assumption is required, namely the viscosity–temperature law

$$\mu T_1/\mu_1 T = C(x,t), \tag{7}$$

discussed by Chapman & Rubesin (1949). This viscosity law is not as accurate a description of the behaviour of μ as the Sutherland relation

$$\frac{\mu}{\mu_1} = \left(\frac{T}{T_1}\right)^{\frac{3}{2}}\left(\frac{T_1+S}{T+S}\right), \tag{8}$$

where S is a constant, but is a more manageable relation to deal with. To minimize the error inherent in (7), the function C is chosen so that the Sutherland relation is satisfied at the wall, thus giving a more precise viscosity coefficient near the wall, where the shear is large. Therefore

$$C(x,t) = \left(\frac{T_w}{T_1}\right)^{\frac{1}{2}}\left(\frac{T_1+S}{T_w+S}\right),$$

and it may be shown that

$$\rho\mu/\rho_l\mu_l = \tilde{p}_1, \quad \mu/\mu_l = H(\xi,\eta)+1.$$

In accordance with boundary-layer theory, the pressure p_1 is assumed to be impressed across the boundary layer. Thus the dimensionless pressure $P = \tilde{p}_1/\gamma$.

This results in the following two coupled equations for Φ and H:

$$\Phi^2\frac{\partial^2\Phi}{\partial\eta^2} + (H+1)\frac{\partial P}{\partial\xi}\frac{\partial\Phi}{\partial\eta} + \left[\gamma(\eta+1-\xi)\frac{\partial P}{\partial\xi} + \frac{\gamma P}{2} - \frac{\partial P}{\partial\xi}\frac{\partial H}{\partial\eta}\right]\Phi = \gamma(\eta+1-\xi)P\frac{\partial\Phi}{\partial\xi}, \tag{9}$$

$$\Phi^2\left[(\gamma-1)+\frac{1}{\sigma}\frac{\partial^2 H}{\partial\eta^2}\right] - \left[\left(1-\frac{1}{\sigma}\right)\Phi\frac{\partial\Phi}{\partial\eta} - (H+1)\frac{\partial P}{\partial\xi}\right] \times\frac{\partial H}{\partial\eta} + (\gamma-1)(\eta+1-\xi)\frac{\partial P}{\partial\xi}(H+1) = \gamma(\eta+1-\xi)P\frac{\partial H}{\partial\xi}, \tag{10}$$

with boundary conditions

(a) on the wall ($\eta = 0$), $\Phi\,\partial\Phi/\partial\eta = \partial P/\partial\xi$, $H = 0$, (11)

(b) at the edge of the boundary layer ($\eta = 2\xi/(\gamma+1)$) $\Phi = 0$, $H = \tilde{h}_1 - 1$. (12)

Equations (9) and (10) are then the equations to be solved simultaneously, subject to the boundary conditions (11) and (12) in the triangular region depicted

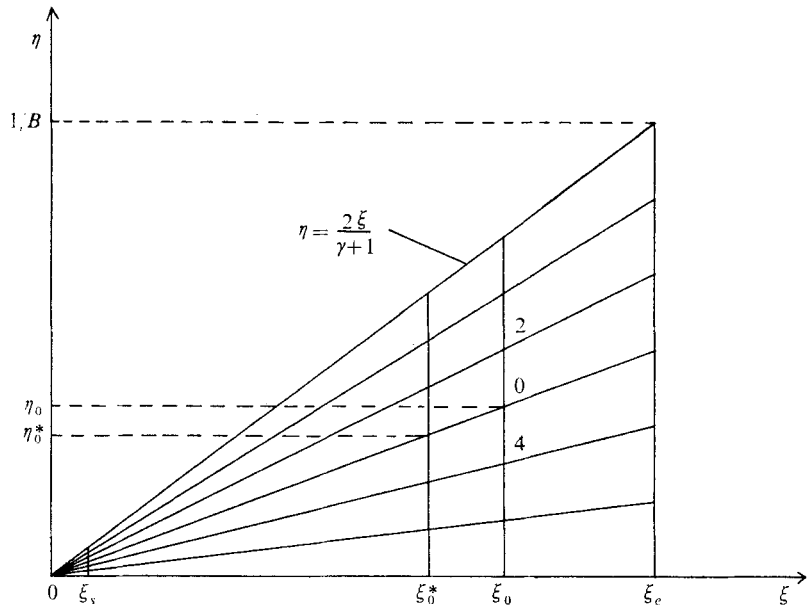

FIGURE 2. The co-ordinate system in the expansion fan ($B = c_{l1}/U_0$).

in figure 2. The variable ξ extends from the front of the expansion fan ($\xi = 0$) to the end at $\xi_e = (\gamma+1)/2B$.

For medium-strength waves $\xi_e < 1$ and the coefficient of the ξ derivative in (9) and (10) is always positive. Thus the solution may be integrated numerically without difficulty by a step-by-step procedure along rays which emanate from the origin $\xi = \eta = 0$ and are tied to a set of equidistant points on the line $\xi = \xi_e$. The solution at some initial station $\xi = \xi_s$ may be determined from the analytical first terms of Cohen's (1957) solution. In the present formulation, Cohen's (1957) solution is

$$\Phi = \frac{2\tilde{p}_1 \xi^{\frac{1}{2}}}{\gamma+1} f'(\lambda) + O(\xi^{\frac{3}{2}}), \quad H = (\tilde{h}_1 - 1)\, g(\lambda) + O(\xi^2), \tag{13}$$

where $f(\lambda) = \frac{1}{2}(\lambda^2+2)\operatorname{erf}(\frac{1}{2}\lambda) - \frac{1}{2}\lambda^2 + (\lambda/\pi^{\frac{1}{2}})\, e^{-\frac{1}{4}\lambda^2}$, $g(\lambda) = f(\sigma^{\frac{1}{2}}\lambda)$.

The variable λ is Cohen's similarity variable, measuring normal distance from the wall. For a particular value of η, say η_0, λ may be evaluated by solving

$$[2\xi_s/(\gamma+1)] f(\lambda) - \eta_0 = 0,$$

by Newton's method. Good approximations to Φ and H at ξ_s may then be obtained from equations (13), provided that ξ_s is small enough. The solution may then be advanced numerically in the ξ direction using a constant ξ grid size h_ξ. The η grid size is constant for fixed ξ and equal to $h_\eta = 2\xi/(m_0 - 1)(\gamma+1)$, where m_0 is the number of grid points taken across the boundary layer including the boundaries. It then remains to describe the numerical technique used to integrate these equations.

2.2. *Numerical methods*

By dividing (9) and (10) by γP it may be seen that these equations are of the form

$$(\eta + 1 - \xi)\,\partial F/\partial \xi = Q, \tag{14}$$

where F and Q are functions of ξ and η, and Q contains first and second derivatives with respect to η. Consider a typical station at $\xi = \xi_0$ and assume that the solution is known along the line $\xi_0^* = \xi_0 - h_\xi$. Consider a typical point on the line $\xi = \xi_0$ at $\eta_0 = ih_\eta$ and denote function value at points $\eta_0 + h_\eta$, η_0 and $\eta_0 - h_\eta$ by subscripts 2, 0 and 4 respectively as in figure 2. By expanding F as a Taylor series about the point (ξ_0, η_0), a finite-difference expression for $\partial F/\partial \xi$ may be obtained as

$$\left.\frac{\partial F}{\partial \xi}\right|_0 \approx \frac{F_0 - F_0^*}{h_\xi} - \frac{\eta_0}{\xi_0}\frac{F_2 - F_4}{2h_\eta}. \tag{15}$$

Here a starred quantity refers to a quantity evaluated on the same ray as the corresponding unstarred quantity but one ξ step to the left at $\xi = \xi_0^*$. Substitution of this expression into (14) and approximation of the η derivatives by ordinary central differences would lead to a fully implicit finite-difference scheme for advancing the solution in the ξ direction, suitable for use with (9) and (10). The difficulty with this is that the error associated with the approximation (15) is only of $O(h_\xi, h_\eta^2)$, and hence an improved scheme similar to the Crank–Nicolson method for parabolic equations was deduced.

A Crank–Nicolson type approximation was derived by Walker† (1971) in connexion with the impulsively started sphere problem. There the time derivative was multiplied by t and in this situation, the ordinary Crank–Nicolson approach is not suitable near $t = 0$. The method is generalized here to deal with the geometry of the present problem, since as $\xi \to 1$ the coefficient of $\partial F/\partial \xi$ in (14) will become small. The double integral of (14) from (ξ_0^*, η_0^*) to (ξ_0, η_0) is evaluated. Omitting the details of the derivation, it may be shown by integrating by parts, expanding F as a Taylor series about the points (ξ_0, η_0) and (ξ_0^*, η_0^*) and using relation (15) that

$$L(F_0 - F_0^*) + M(F_2 - F_4) + N(F_2^* - F_4^*) \approx Q_0 + Q_0^*, \tag{16}$$

where

$$L = 1 + (2/h_\xi)\,[\tfrac{1}{2}(\eta_0 + \eta_0^*) + 1 - \xi_0],$$
$$M = (1/h_\xi h_\eta)\,[\tfrac{1}{3}\theta^2 - \tfrac{1}{2}\theta(\eta_0 + 1 - \xi_0)],$$
$$N = -(1/h_\xi h_\eta^*)\,[\tfrac{1}{3}\theta^2 + \tfrac{1}{2}\theta(\eta_0^* + 1 - \xi_0^*)].$$

Here $\theta = \eta_0 - \eta_0^*$ is the difference between two successive ordinates on a ray and $\theta = \eta_0 h_\xi/\xi_0$. The error associated with the approximation (16) is of

$$O[h_\xi^2, \theta h_\xi, \theta^2, \theta h_\eta^2/h_\xi, \theta^3/h_\xi].$$

The grid sizes h_ξ and h_η were chosen so that $h_\eta < h_\xi$ and for $\gamma > 1$, $\theta < h_\xi$. Thus (16) gives a more accurate approximation to (14) than (15) would do and this was used to advance the solution for Φ and H in the ξ direction.

† See also Dennis & Walker (1972).

The η derivatives which appear in $Q(\xi, \eta)$ (here Q is equal to $(\gamma P)^{-1}$ times the left-hand side of (9) or (10)) were approximated by central differences according to

$$\left.\frac{\partial^2 F}{\partial \eta^2}\right|_0 = \frac{F_2 - 2F_0 + F_4}{h_\eta^2} + O(h_\eta^2), \quad \left.\frac{\partial F}{\partial \eta}\right|_0 = \frac{F_2 - F_4}{2h_\eta} + O(h_\eta^2), \tag{17}$$

thus giving a set of finite-difference equations for the unknown function values on $\xi = \xi_0$. These equations may be written at a typical grid point at (ξ_0, η_0) as

$$b_0 \Phi_2 + a_0 \Phi_0 + c_0 \Phi_4 = d_0, \tag{18}$$

for Φ, where

$$a_0 = -2\Phi_0^2 + h_\eta^2[\Gamma'(\eta_0 + 1 - \xi_0) + \tfrac{1}{2}\Gamma] - (h_\eta/\gamma)\,\Gamma'\tilde{\mu}\delta H_0 - h_\eta^2 \Gamma L,$$

$$b_0 = 2\Phi_0^2 - c_0 = \Phi_0^2 + (h_\eta/2\gamma)\,\Gamma'(H_0 + 1) - h_\eta^2 \Gamma M,$$

$$d_0 = -\frac{\Gamma h_\eta^2}{\Gamma^* h_\eta^{*2}}\left[\left\{\Phi_0^{*2}\delta^2 + \frac{1}{\gamma}h_\eta^*\Gamma^{*\prime}(H_0^* + 1)\tilde{\mu}\delta + h_\eta^{*2}(\eta_0^* + 1 - \xi_0^*)\,\Gamma^{*\prime} + \tfrac{1}{2}h_\eta^{*2}\Gamma^* - \frac{1}{\gamma}h_\eta^*\Gamma^{*\prime}\tilde{\mu}\delta H_0^*\right\}\Phi_0^*\right] + 2h_\eta^2\Gamma N\tilde{\mu}\delta\Phi_0^* - L\Gamma h_\eta^2\Phi_0^*,$$

where $\Gamma = \gamma P$ and the prime indicates differentiation with respect to ξ. Here the quantities $\tilde{\mu}$ and δ are the averaged-central-difference and central-difference operators respectively in the η direction. A set of difference equations similar to (18),

$$\bar{b}_0 H_2 + \bar{a}_0 H_0 + \bar{c}_0 H_4 = \bar{d}_0, \tag{19}$$

may be obtained for H, using (10), (16) and (17).

Equations (18) and (19) thus give a set of nonlinear coupled difference equations at all interior points ($\eta = h, 2h, \ldots, (m_0 - 2)h$) at $\xi = \xi_0$. From (11) and (12), H and Φ are known at $\eta = (m_0 - 1)h_\eta$ while H is known on $\eta = 0$. The derivative boundary condition on Φ at $\eta = 0$ requires some care however. Denote function values at grid points at $\xi = \xi_0$, $\eta = -h$, 0, h, $2h$, $3h$ by subscripts -1, w, 1, 2, 3 respectively. The obvious way of handling the first of conditions (11) at the wall is to approximate the first derivative by a central difference across the wall, according to the second of equations (17). This gives

$$\Phi_{-1} = \Phi_1 - \frac{2h_\eta}{\Phi_w}\frac{\partial P}{\partial \xi} + O(h_\eta^3). \tag{20}$$

The differential equation (9) could then be assumed to hold on the wall and could be approximated by (18) on $\eta = 0$ as well as at all interior points. Equation (20) would then be used to eliminate Φ_{-1} from the difference equation on $\eta = 0$. The difficulty with this approach is that, when (20) is substituted into an expression for $\partial^2\Phi/\partial\eta^2$ similar to the first of equations (17), the resulting accuracy of the approximation to the second derivative will only be of $O(h_\eta)$. While this may be acceptable in a region where Φ and its derivatives are becoming small, it is not felt to be appropriate for use with the Crocco equation where the shear is largest near the wall. To retain an $O(h_\eta^2)$ accuracy near the wall, a finite-difference approximation of $O(h_\eta^3)$ must be used for the derivative condition. The sloping difference formula

$$\left.\frac{\partial \Phi}{\partial \eta}\right|_w = \frac{-11\Phi_w + 18\Phi_1 - 9\Phi_2 + 2\Phi_3}{6h_\eta} + O(h_\eta^3) \tag{21}$$

P_R	B	ξ_e	m_0	n_0^*	$h_\xi = \xi_s$
2	4·0402	0·2970	81	73	$4{\cdot}13 \times 10^{-3}$
			161	145	$2{\cdot}06 \times 10^{-3}$
6	1·5639	0·7673	81	161	$4{\cdot}80 \times 10^{-3}$
			161	321	$2{\cdot}40 \times 10^{-3}$
10	1·2177	0·9855	81	225	$4{\cdot}40 \times 10^{-3}$
			161	449	$2{\cdot}20 \times 10^{-3}$

TABLE 1. Parameters of the calculations in the expansion wave

was used in the boundary condition, and substitution in the first of equations (11) yields

$$11\Phi_w = 18\Phi_1 - 9\Phi_2 + 2\Phi_2 - \frac{6h_\eta}{\Phi_w}\frac{\partial P}{\partial \xi} + O(h_\eta^4). \tag{22}$$

The difference equations for Φ and H at ξ_0 defined at all interior points were solved by the direct method described by Rosser (1967) in which the derivative condition (22) is easily incorporated. Since the difference equations (18) and (19) are coupled and nonlinear (as well as the boundary condition (22)), iteration is necessary at each ξ_0. This was done by the following procedure. Assume that the iterate with superscript j has been completed and solutions $\Phi^{(j)}(\xi_0, \eta)$ and $H^{(j)}(\xi_0, \eta)$ have been produced. These were then used to approximate the coefficients of the difference equations (18) and (19) as well as the last term on the right-hand side of (22). This redefined set of difference equations was then used to produce the iterate with superscript $j+1$. A flip-flop technique was employed whereby three iterations or less were performed, depending on whether or not convergence was achieved, on the equation for either Φ or H before turning to the other equation. At any stage, the most recently available information for the coefficients of (18) and (19) was used. This process was continued until ultimately convergence was obtained, which was decided by the test

$$\left|1 - \Phi^{(j)}(\xi_0, \eta_i)/\Phi^{(j+1)}(\xi_0, \eta_i)\right|, \left|1 - H^{(j)}(\xi_0, \eta_i)/H^{(j+1)}(\xi_0, \eta_i)\right| < 10^{-5}, \tag{23}$$

for all $\eta_i = ih_\eta$ $(i = 1, 2, \ldots, (m_0 - 2))$. The value of Φ on $\eta = 0$ was then obtained from (22) and the solution advanced to $\xi = \xi_0 + h_\xi$, where the process was continued.

Three cases corresponding to $P_R = 2$, 6 and 10 for an air–air shock tube with Prandtl number $\sigma = 0{\cdot}73$, specific heat ratio $\gamma = 1{\cdot}4$ and constant wall temperature T_w were considered. This gas was chosen partly with the view of avoiding the mathematically simpler case $\sigma = 1$. Two sets of grid sizes were used for each case as a check on the accuracy and agreement was excellent. The parameters of the calculations, which were carried out on the University College London I.B.M. 360–65 in double precision, are given in table 1. The number of grid points between and including $\xi = 0$ and $\xi = \xi_e$ is denoted by n_0^*. Since Φ and H are independent of B and since the solutions in the fan were carried out independently for each case, an additional check on the numerical accuracy was obtained in the range of ξ where the solutions overlap. Convergence at each ξ step was very rapid, requiring at most five iterations each for Φ and H.

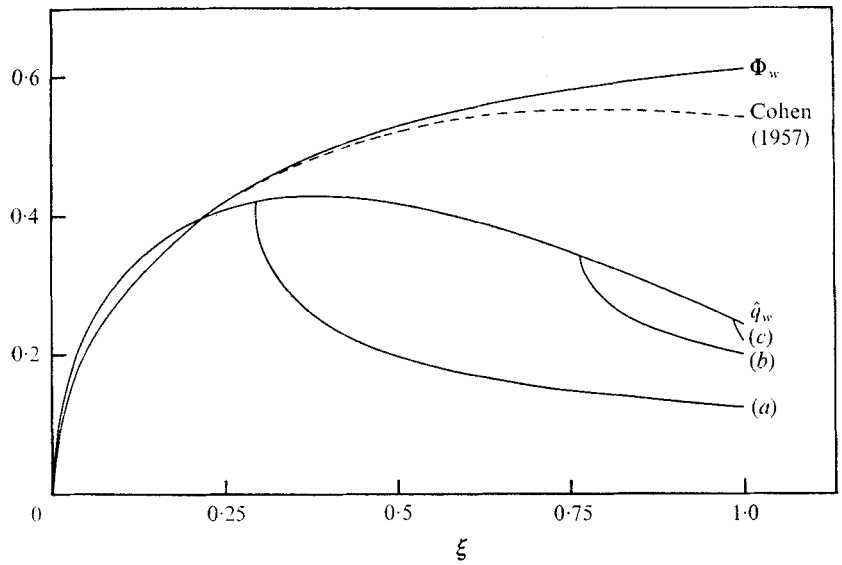

FIGURE 3. Wall shear stress Φ_w and heat-transfer coefficient $\hat{q}_w$ in the expansion fan; departure of $\hat{q}_w$ in the L region for (*a*) $P_R = 2$, (*b*) $P_R = 6$, (*c*) $P_R = 10$.

2.3. *Calculated results*

The dimensionless shear stress Φ_w on the tube wall is plotted in figure 3 in the range $0 \leqslant \xi \leqslant 1$ and it is a monotonically increasing function of ξ throughout the fan. As a comparison Cohen's (1957) series solution (which is for $\sigma = 0{\cdot}72$) is also given and it may be seen that, as he conjectured, his results are valid in the range $0 \leqslant \xi \lesssim 0{\cdot}3$, being virtually identical with the present solution. If the heat transferred per unit time per unit surface are from the wall to the fluid is denoted by q_w, then

$$q_w = -(\mu_w/\sigma)(\partial h/\partial y)_w.$$

A dimensionless coefficient of heat transfer $\hat{q}_w$ may be defined as

$$\hat{q}_w = \frac{q_w}{c_l^2}\left(\frac{t}{\rho_l \mu_l}\right)^{\frac{1}{2}} = -\frac{\Phi_w}{\sigma(\gamma-1)}\left.\frac{\partial H}{\partial \eta}\right|_{\eta=0}, \tag{24}$$

and this is plotted in figure 3 for a fan that extends all the way to the diaphragm (at $\xi = 1$). As ξ increases from zero, $\hat{q}_w$ increases monotonically, reaching a maximum at about $\xi \approx 0{\cdot}38$, and then decreases until $\xi = 1$. Again this behaviour is in general agreement with Cohen's (1957) solutions. Since the present solutions do not show any radical departures from Cohen's (1957) work and are a logical continuation of his solutions, the flow in the fan is not discussed further here.

At this stage the solution is now known at the end of the fan and may be used (for the three cases considered) as a boundary condition on the left edge of the L region. The problem is now to proceed through the L region to the diaphragm.

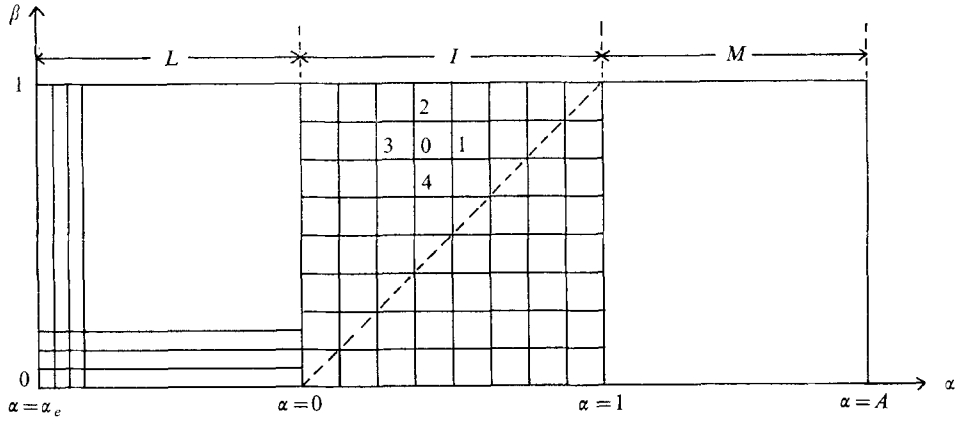

FIGURE 4. Co-ordinate system and grid structure in the L, I and M regions.

3. The L region

3.1. *Basic equations*

At the end of the fan the pressure gradient vanishes. The pressure (equal to p_0) and the free-stream velocity (equal to U_0) are constant throughout the L, I and M regions. The normalized free-stream enthalpy is constant and equal to $\mathscr{H}_1$ in the L and I regions and $\mathscr{H}_0$ in the M region ($\mathscr{H}_1 < \mathscr{H}_0$). The viscosity law (7) may be written as $\rho\mu = \rho_w\mu_w$ = constant, where w indicates a quantity evaluated at the wall; this law has the effect of decoupling (1) and (2) when the pressure gradient is zero. The appropriate similarity variables in the L, I and M regions are

$$\left.\begin{aligned} \alpha = x/U_0 t, \quad \beta = u/U_0, \quad \tilde{\Omega} = \rho_w U_0^2 t/\mu_w, \\ \tau = \rho_w U_0^2 \phi \tilde{\Omega}^{-\frac{1}{2}}, \quad H = (h-h_w)/h_w. \end{aligned}\right\} \tag{25}$$

Assuming that ϕ and H are independent of $\tilde{\Omega}$, in terms of these variables (1) and (2) become

$$\phi^2 \partial^2\phi/\partial\beta^2 + \tfrac{1}{2}\phi = (\beta-\alpha)\partial\phi/\partial\alpha, \tag{26}$$

$$\phi^2\left\{\frac{(\gamma-1)}{B^2} + \frac{1}{\sigma}\frac{\partial^2 H}{\partial\beta^2}\right\} - \left(1-\frac{1}{\sigma}\right)\phi\frac{\partial\phi}{\partial\beta}\frac{\partial H}{\partial\beta} = (\beta-\alpha)\frac{\partial H}{\partial\alpha}, \tag{27}$$

with boundary conditions

$$\partial\phi/\partial\beta = H = 0 \quad \text{at} \quad \beta = 0, \tag{28}$$

$$\phi = 0, \quad H = \mathscr{H}_1 \quad \text{or} \quad \mathscr{H}_0 \quad \text{at} \quad \beta = 1. \tag{29}$$

The domain of the solution is now the rectangular region depicted in figure 4.

At this stage the solution for Φ and H is known at $\alpha_e = -B(1-\xi_e)$. The transformation into the present similarity variables is

$$\phi = B\{1-(\gamma-1)/2B\}^{-\gamma/(\gamma-1)}\Phi, \quad \beta = B\eta, \tag{30}$$

and the problem is to integrate the solution from $\alpha = \alpha_e$ to the diaphragm $\alpha = 0$. This was done numerically be a step-by-step procedure which is now briefly described.

P_R	α_e	m_0	n_0	h_1
2	−2·8402	81	171	$1{\cdot}67\times10^{-2}$
		161	341	$8{\cdot}35\times10^{-3}$
6	−0·3639	81	81	$4{\cdot}55\times10^{-3}$
		161	161321	$1{\cdot}14\times10^{-3}$
10	−0·01772	81	33	$5{\cdot}54\times10^{-4}$
		161	65129	$1{\cdot}38\times10^{-4}$

TABLE 2. Parameters of the calculations in the L region

3.2. *Numerical procedure*

Equations (26) and (27) are both of the form

$$(\beta-\alpha)\,\partial F/\partial\alpha = Q, \tag{31}$$

where Q involves β derivatives of F. By holding β constant and integrating (31) from α_0^* to α_0, where $\alpha_0^* = \alpha_0 - h_1$ and h_1 is the α grid size, it may be shown that

$$(\beta-\alpha_0+\tfrac{1}{2}h_1)\,(F_0-F_0^*) = \tfrac{1}{2}h_1(Q_0+Q_0^*)+O(h_1^3), \tag{32}$$

where the star indicates a quantity evaluated at α_0^*. If the β derivatives of F in Q are approximated by central differences according to (17), then tridiagonal matrix problems similar to (18) and (19) may be formulated for ϕ and H from (26) and (27) respectively, for the unknown function values at interior points $\beta = ih_2$ $(i = 1, 2, \ldots, (m_0-2))$ at $\alpha = \alpha_0$, assuming that the solution is known at $\alpha = \alpha_0^*$. Here h_2 is the β grid size. Thus (32) provides an implicit method of advancing the solution in the α direction. Since the procedure is similar in many respects to that described in §2.2, it will not be described in detail here. The derivative boundary condition on ϕ at $\beta = 0$ was approximated by a relation analagous to (22) (with $\partial P/\partial\xi = 0$). Since (26) is nonlinear, the difference equations (which are similar to (18)) are nonlinear and some iteration is required at each α step. For the parameters quoted in table 2, convergence (decided by a test analogous to (23)) occurred in two to five iterations. Equation (27) is linear in H and may be solved directly once ϕ is known.

Two β grid sizes of $h_2 = 0{\cdot}0125$ and $0{\cdot}00625$ corresponding to $m_0 = 81$ and 161 points across the boundary layer were used in the L region. This is a region of some numerical difficulty, particularly near $\alpha = \alpha_e$, and very fine α grid sizes had to be used to obtain close agreement between successive solutions at a particular value of α, agreement at $\alpha = 0$ being of most importance. The various α grid sizes used are given in table 2. The number of grid points used between and including $\alpha = \alpha_e$ and $\alpha = 0$ is denoted by n_0 and the quoted value h_1 of the α grid size corresponds to the finest grid size used for a particular value of m_0. The difficulty in the L region is centred mainly near the end of the fan and the reason for this may be inferred from a comparison of (9) and (10) and (26) and (27). The removal of the pressure gradient at the end of the fan causes a discontinuity in the derivatives $\partial\phi/\partial\alpha$ and $\partial H/\partial\alpha$ at $\alpha = \alpha_e$ and also a discontinuous change in

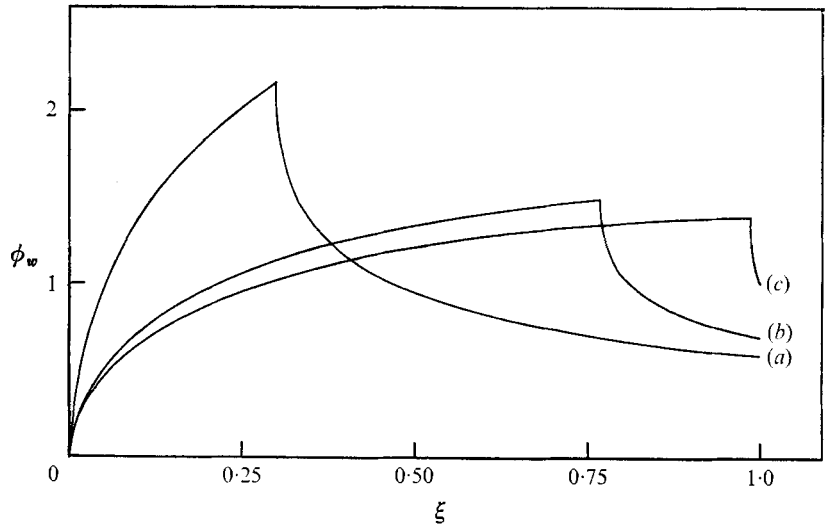

FIGURE 5. Wall shear stress in the E and L regions for (*a*) $P_R = 2$, (*b*) $P_R = 6$, (*c*) $P_R = 10$.

the boundary condition for ϕ in the wall. The nature of the solution for ϕ and H near $\alpha = \alpha_e$ is examined in the appendix and it is clear from the results given there that in order to obtain an accurate numerical solution in the region $\alpha = \alpha_e +$ fine grid sizes h_1 must be used. With this is mind, the first α step from $\alpha = \alpha_e$ (as given in table 2) was further subdivided into fifty equal intervals. This procedure produced good agreement of the various solutions in the L region.

3.3. *Calculated results*

The non-dimensional shear stress ϕ_w on the wall is plotted in figure 5 versus the variable ξ for $\xi \geqslant \xi_e$. To illustrate clearly the discontinuity in $\partial\phi/\partial\xi$, ϕ_w is also plotted for $\xi < \xi_e$ in the expansion fan (where ϕ_w is just a constant times Φ_w). It is apparent that, as P_R increases, the drop in ϕ_w becomes more severe at the end of the fan. The same type of behaviour occurs for the heat-transfer coefficient $\hat{q}_w$ and in figure 3 the curves labelled (*a*), (*b*) and (*c*) illustrate the departure from the fan solution of $\hat{q}_w$ in the L region for the three cases considered.

The physical variable y is retrieved by integration of $\tau = \mu\,\partial u/\partial y$, and

$$y\left(\alpha, \frac{u}{U_0}\right) = \int_0^\beta \left(\frac{t}{\rho_w \mu_w}\right)^{\frac{1}{2}} \frac{\mu(\alpha,\zeta)}{\phi(\alpha,\zeta)}\, d\zeta. \tag{33}$$

Defining a dimensionless ordinate z by

$$z\left(\alpha, \frac{u}{U_0}\right) = \frac{y}{(\nu_w t)^{\frac{1}{2}}} = \int_0^\beta \frac{H(\alpha,\zeta)+1}{\phi(\alpha,\zeta)}\, d\zeta, \tag{34}$$

a dimensionless boundary-layer thickness $\delta^* = z(\alpha, 0{\cdot}975)$ may be defined as that ordinate at which the velocity u achieves 97·5% of the free-stream value. The boundary-layer thickness δ^* is plotted in figure 6 in the range $0 \leqslant \xi \leqslant 1$ for the three cases considered. At the end of the fan $\partial\delta^*/\partial\xi$ is discontinuous and the

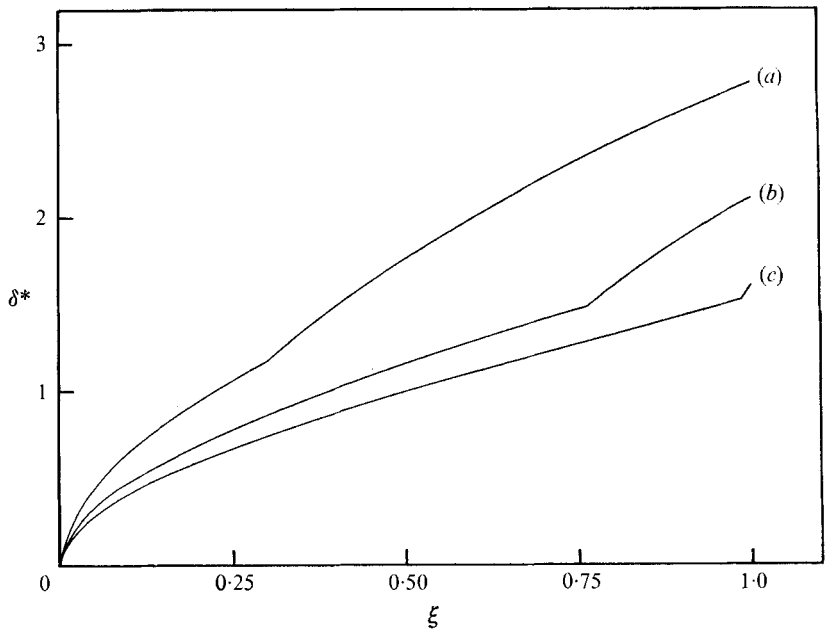

FIGURE 6. Boundary-layer thickness δ^* in the E and L regions for (a) $P_R = 2$, (b) $P_R = 6$, (c) $P_R = 10$.

boundary layer thickens at a faster rate upon passing from the E to the L region. The reason for this behaviour as well as that of ϕ_w and $\hat{q}_w$ at the end of the fan is due to the sudden removal of the pressure gradient; this is discussed more fully in the appendix.

Lastly, it may be seen that the flow in the E–L region is very different from that predicted by the infinitely thin expansion wave solution of Mirels (1956) which was used by Ban & Kuerti (1969) in their study of the I region. The important question, however, as regards the interaction region is how the solutions agree at the diaphragm. The case Ban & Kuerti (1969) considered was for $P_R = 1{\cdot}35$ and $\sigma = 1$ and this case was briefly considered by the present method. It was found that, although the solutions do not agree throughout most of the E–L region, agreement is reasonably close at the diaphragm. This indicates that for very weak waves the assumption of a zero-thickness expansion wave gives a good approximation to the flow at the diaphragm. In this case the downstream influence of the fan seems to be slight.

4. The M region

In the M region, which extends from $\alpha = 1$ to $\alpha = A$, the problem coincides with the problem considered by Mirels (1955). Here, as Stewartson (1964) has pointed out, the solution is independent of conditions in the I region. The variables may be separated according to

$$\phi(\alpha,\beta) = \left(\frac{A-1}{A-\alpha}\right)^{\frac{1}{2}} M(\beta), \quad H(\alpha,\beta) = H_M(\beta), \tag{35}$$

where
$$MM'' + \frac{1}{2}\left(\frac{A-\beta}{A-1}\right) = 0, \quad \text{with} \quad M'(0) = M(1) = 0, \tag{36}$$

$$M\left\{\frac{\gamma-1}{B^2} + \frac{1}{\sigma}H''_M\right\} - M'H'_M\left(1-\frac{1}{\sigma}\right) = 0, \quad \text{with} \quad H_M(0) = 0, \quad H_M(1) = \mathscr{H}_0, \tag{37}$$

where $\mathscr{H}_0$ is the constant normalized free-stream enthalpy, which is strictly greater than the value $\mathscr{H}_1$ in the L and I regions.

If the expansion wave is treated as being infinitely thin, a reduction similar to equations (35) may be made in the L region and equations similar to (36) and (37) obtained. This was done by Ban & Kuerti (1969), who then linearized equation (36) (and a similar one for the L region) by expanding M and H_M in a power series in A^{-1}. A consistent linearization scheme was then used to solve the problem in the I region. In their case $A = 9{\cdot}95$ but since in the present paper cases where A is much smaller are considered this approach was not thought to be profitable.

It is required, then, to solve the ordinary differential equations (36) and (37) for a particular value of A. Equation (36) may be written as

$$M''(\beta) = \kappa(\beta), \quad \text{where} \quad \kappa(\beta) = -\frac{1}{2M(\beta)}\frac{(A-\beta)}{(A-1)}. \tag{38}$$

Denote function values at grid points $\beta_0 - h$, β_0 and $\beta_0 + h$, where β_0 is a typical internal mesh point and h is the numerical grid size, by subscripts 4, 0 and 2 respectively. The finite-difference approximation discussed by Fox (1957, p. 68),

$$M_2 - 2M_0 + M_4 = \frac{h^2}{12}(\kappa_2 + 10\kappa_0 + \kappa_4) + O\left(\frac{\delta^6 M_0}{240}\right), \tag{39}$$

was used at all interior grid points, except at the point adjacent to the boundary, $\beta = 1$, where $\kappa(1)$ is undefined. At this point, (36) was approximated by the difference formula given by Fox (1957, p. 18) as

$$M_2 - 2M_0 + M_4 = h^2\kappa_0 + \tfrac{1}{12}(\nabla^4 + \nabla^5)M_2 + O(\tfrac{13}{180}\nabla^6 M_2), \tag{40}$$

where ∇ is the backward-difference operator in the β direction. Equation (40) is multiplied by M_0 and thus, with (39), a tridiagonal matrix problem is obtained for the internal function values at all internal points. This was solved by an iterative procedure by the direct method described by Rosser (1967). The derivative boundary condition in (36) was approximated by

$$(\Delta - \tfrac{1}{2}\Delta^2 + \tfrac{1}{3}\Delta^3 - \tfrac{1}{4}\Delta^4 + \tfrac{1}{5}\Delta^5)M(0) = 0 + O(\tfrac{1}{6}\Delta^6 M(0)), \tag{41}$$

where Δ is the forward-difference operator. Since $\kappa(\beta)$ in (39) and the second term on the right-hand of (40) contain unknown internal function values, some iteration is necessary to obtain a solution for a given A. It was found that by averaging two successive iterates, by taking their arithmetic mean, a solution for $M(\beta)$ could be obtained in ten to fifteen iterations (employing a convergence criterion similar to the first of (23)). Three grid sizes of $h = 0{\cdot}05$, $0{\cdot}025$ and $0{\cdot}0125$ were used as a check on the accuracy.

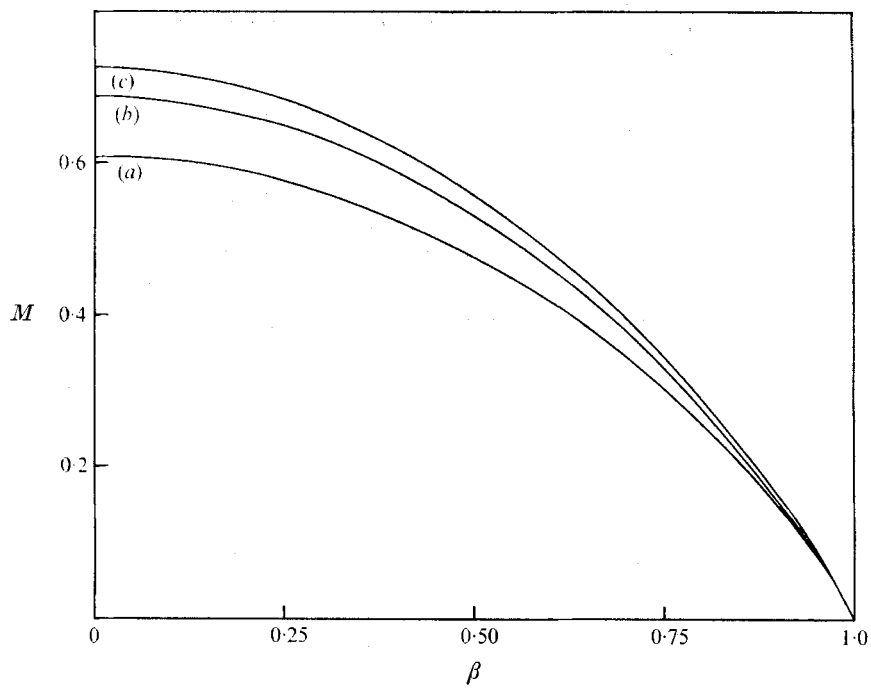

FIGURE 7. $M(\beta)$ for (a) $P_R = 2$, (b) $P_R = 6$, (c) $P_R = 10$.

Once a solution for $M(\beta)$ had been obtained (37) was solved numerically for $H_M(\beta)$. Using ordinary central-difference approximations, a tridiagonal matrix problem may be formulated for all internal values of H_M; this was then solved directly. Once a solution had been obtained for $H_M(\beta)$ difference corrections of

$$\left[\frac{M(\beta)}{12\sigma}\delta^4 - \frac{h}{6}\left(1-\frac{1}{\sigma}\right)M'(\beta)\tilde{\mu}\delta^3\right]H_M(\beta)$$

were added to the original difference equations as homogeneous correction terms, in accordance with the method described by Fox (1957, p. 67). This was done at all interior points except those adjacent to the boundaries, where sloping difference corrections were used. Convergence of this iterative scheme, decided by a test similar to the second of (23), is very rapid. In this manner the ultimate truncation error was of $O(h^4)$.

The functions $M(\beta)$ are plotted in figure 7 for the three cases considered. Some test cases of large A were considered by the present method and good agreement was obtained with the linearized solutions of Ban & Kuerti (1969). The character of the solution in the M region has been well discussed by Mirels (1955) and will not be described in detail here.

5. The interaction region

5.1. *Numerical scheme*

At this stage the solution is known throughout the shock tube except in the interaction region I, and in particular it is known as $\alpha \to 0-$ and as $\alpha \to 1+$. The nature of the problem in the I region now becomes more apparent. Numerical marching techniques, whether started from $\alpha = 0$ or $\alpha = 1$, will fail since the coefficient of the α derivative in (26) and (27) vanishes and changes sign in the I region where $0 \leqslant \alpha \leqslant 1$. In the I region, where $\beta > \alpha$ the preferred direction is the $+\alpha$ direction as the influence is due to the driver gas whereas where $\beta < \alpha$ the preferred direction is the $-\alpha$ direction and the influence is due mainly to the boundary layer created by the passage of the shock. Since the solution in the I region must match the solution at $\alpha = 0$ and $\alpha = 1$, the problem must be treated as a boundary-value problem. This was recognized by Lam & Crocco (1958) and they attempted to prove that the solution in the I region is unique with boundary conditions specified at $\alpha = 0$ and $\alpha = 1$.

In the present problem the boundary conditions for the I region are the solution in the M region at $\alpha = 1$ and the solution in the L region at $\alpha = 0$. The problem is then to solve (26) and (27) in the square I region depicted in figure 4 with boundary conditions (28) and (29) on $\beta = 0, 1$ respectively and H and ϕ known on $\alpha = 0, 1$.

With the ultimate view of making the numerical scheme convergent, it is convenient to work in terms of the perturbation function $\zeta(\alpha, \beta)$, where

$$\zeta(\alpha, \beta) = \phi(\alpha, \beta) - \phi_0(\beta). \tag{42}$$

Here

$$\phi_0(\beta) = (1/\pi^{\frac{1}{2}}) \exp\{-\mathrm{fre}^2 \beta\} \tag{43}$$

is the Rayleigh (1911) solution expressed in Crocco variables. Ban & Kuerti (1969) refer to ϕ_0 as the zeroth-order shear stress and the function $\mathrm{fre}(\beta)$, as termed by these authors, is the inverse error function. Equation (26) now becomes

$$E\, \partial^2\zeta/\partial\beta^2 - F\zeta = (\beta - \alpha)\, \partial\zeta/\partial\alpha, \tag{44}$$

where

$$E = (\phi_0 + \zeta)^2, \quad F = \tfrac{1}{2}\{1 + \pi^{\frac{1}{2}} \zeta \exp(\mathrm{fre}^2 \beta)\}, \tag{45}$$

and ζ satisfies the same boundary conditions as ϕ on $\beta = 0, 1$.

A square grid in the I region with grid size h was used. Using the Southwell system (indicated in figure 4) to number grid points about a typical point 0 in the mesh, a straightforward central-difference approximation to (44) would be

$$E_0(\zeta_2 - 2\zeta_0 + \zeta_4) - h^2 F_0 \zeta_0 = \tfrac{1}{2}h(\beta - \alpha)(\zeta_1 - \zeta_3). \tag{46}$$

Now $E \geqslant 0, F \geqslant 0$ and we suppose that E and F are known. The difficulty with the system of equations (46) is that in general they are not diagonally dominant in the sense described by Varga (1962, p. 23) and hence an iterative method of solution based on this approximation is likely to diverge. The situation may be rectified however by replacing the α derivative in (44) by a simple forward- or backward-difference approximation depending on the sign of $\beta - \alpha$. This technique was first suggested by Spalding (1967) and later by Greenspan (1968) in studies of the Navier–Stokes equations and has been used by many others since then. Dennis

(1972) recognized that this technique could be applied to singular-parabolic equations and solved the problem of an impulsively started, semi-infinite flat plate in this manner. In the present problem the technique is as follows. The finite-difference approximation to (44) is

$$E_0(\zeta_2 - 2\zeta_0 + \zeta_4) - h^2 F_0 \zeta_0 - h(\beta - \alpha) Q = C_0, \tag{47}$$

where

$$Q = \begin{cases} \zeta_0 - \zeta_3 & \text{if} \quad (\beta - \alpha) > 0, \\ \zeta_1 - \zeta_0 & \text{if} \quad (\beta - \alpha) < 0, \end{cases}$$

and C_0 is a correction term. If the correction term C_0 is neglected, (47) defines a set of difference equations at all interior points in the I region which is everywhere diagonally dominant. It should be noted that this difference scheme takes differences of the α derivative in the preferred direction throughout the I region.

As in § 2.2 the derivative boundary condition on ζ at $\beta = 0$ must be treated with some care. Consider equation (47) at the grid point adjacent to the wall $\beta = 0$. Approximation of the derivative condition by a sloping-difference formula similar to (21) indicates that the value ζ_4 of ζ on the wall is related to the interior points by

$$\zeta_4 = \tfrac{1}{11}(18\zeta_0 - 9\zeta_2 + 2\zeta_5), \tag{48}$$

where ζ_5 is the value of ζ at $\beta = 3h$ and the truncation error is of $O(h^4)$. Substitution of this into (47) gives

$$\tfrac{2}{11} E_0(-2\zeta_0 + \zeta_2 + \zeta_5) - h^2 F_0 \zeta_0 - h(\beta - \alpha)(\zeta_1 - \zeta_0) = C_0^* \tag{49}$$

as the typical difference equation along the line $\beta = h$, and diagonal dominance on $\beta = h$ is preserved. Here C_0^* is a correction term. Neglecting for the moment the correction terms in (47) and (49), the resulting difference equations defined at all internal mesh points were solved by the iterative Gauss–Seidel procedure (Varga 1962) in the following manner. Suppose that the iterate with superscript j has been completed. Then approximations to E and F were obtained and the mesh was swept along lines of constant α starting with $\alpha = h$, to produce the iterate with superscript $j+1$. This process was continued until convergence, decided by the test

$$|1 - \zeta^{(j)}/\zeta^{(j+1)}| < 10^{-4}, \tag{50}$$

for all internal points, was obtained. It should be noted that, for this problem, this test of convergence is a more stringent one than requiring the absolute value of the difference of two successive iterates to be less than 10^{-5}. Having obtained a solution for ζ in this manner, the values of ζ on the wall were obtained from (48). Once ζ is known, ϕ is known and (27) may be solved for $H(\alpha, \beta)$. A finite-difference scheme similar to (47) was used to approximate (27) as

$$E_0^*(H_2 - 2H_0 + H_4) - \tfrac{1}{2} h F_0^*(H_2 - H_4) + h^2 G_0^* - h(\beta - \alpha) Q^* = D_0, \tag{51}$$

where

$$Q^* = \begin{cases} H_0 - H_3 & \text{if} \quad \beta - \alpha > 0, \\ H_1 - H_0 & \text{if} \quad \beta - \alpha < 0, \end{cases}$$

$$E^* = \frac{\phi^2}{\sigma}, \quad F^* = \left(1 - \frac{1}{\sigma}\right) \phi \frac{\partial \phi}{\partial \beta}, \quad G^* = \frac{(\gamma - 1)}{B^2} \phi^2,$$

and D_0 is a correction term. Neglect of the correction term yields a set of diagonally dominant difference equations at all internal mesh points; H is known on $\beta = 0$ and $\beta = 1$ from (28) and (29) respectively. A successive over-relaxation scheme was found to produce faster convergence than Gauss–Seidel iteration. Two grid sizes of $h = 0{\cdot}05$ and $h = 0{\cdot}025$ were used for both the ϕ and H equations and over-relaxation factors of $\omega = 1{\cdot}4$ and $1{\cdot}5$ respectively seemed to give rapid convergence for the H equation. Convergence was decided by a test similar to equation (50).

In order to avoid very small grid sizes in the I region, which invariably lead to large computing times, it is necessary to make some allowance for higher order difference corrections. It may be shown from the formulae given by Fox (1957, p. 18) that, for all points in the interior and not adjacent to the boundaries $\beta = 0$ and $\beta = 1$, the leading difference correction terms in C_0 in (47) are

$$\tfrac{1}{12}\{E_0\delta^4 + 6h|\beta-\alpha|\,\delta_1^2\}\zeta_0. \tag{52}$$

Here δ and δ_1 are the central-difference operators in the β and α directions respectively. For points adjacent to the boundary $\beta = 1$, to avoid considering points outside the region, the leading terms in C_0 are

$$\tfrac{1}{12}\{E_0(\nabla^3 + \nabla^4)\,\Delta + 6h|\beta-\alpha|\,\delta_1^2\}\zeta_0, \tag{53}$$

where ∇ and Δ are the backward- and forward-difference operators in the β direction respectively. For the points adjacent to the boundary $\beta = 0$, incorporating the higher order derivative formula (41), the leading terms in the difference correction C_0^* in (49) are

$$\tfrac{1}{12}\{E_0(\Delta^3 - \Delta^4)\,\nabla + (12E_0/1507)\,(162\Delta - 243\Delta^2 + 297\Delta^3 - 132\Delta^4) + 6h|\beta-\alpha|\,\delta_1^2\}\zeta_0. \tag{54}$$

Having obtained a converged solution for ζ by neglecting the corrections C_0 and C_0^*, the leading terms in these corrections were calculated and added to the difference equations (47) and (49) as homogeneous correction terms. The iterative scheme for ζ was then continued, the corrections being updated from time to time until ultimately overall convergence was obtained. The value of ζ on the wall was then obtained by inversion of (41) as

$$\zeta(\alpha, 0) = \tfrac{1}{137}\{137 - 77\Delta + 47\Delta^2 - 27\Delta^3 + 12\Delta^4\}\zeta(\alpha, h). \tag{55}$$

The derivative $\partial\phi/\partial\beta$ for use in the enthalpy equation was then estimated using central- and sloping-difference formulae which are accurate to $O(h^4)$.

The leading terms in the difference corrections D_0 in the H equation (51) are

$$\tfrac{1}{12}\{E_0^*\,\delta^4 - 2hF_0^*\,\tilde{\mu}\delta^3 + 6h|\beta-\alpha|\,\delta_1^2\}H_0, \tag{56}$$

for all points not adjacent to $\beta = 0$ and $\beta = 1$. For points adjacent to $\beta = 0$ the leading terms in D_0 are

$$\tfrac{1}{12}\{E_0^*(\Delta^3 - \Delta^4)\,\nabla + hF_0^*(-2\Delta^2 + \Delta^3)\,\nabla + 6h|\beta-\alpha|\,\delta_1^2\}H_0, \tag{57}$$

and for points adjacent to $\beta = 1$,

$$\tfrac{1}{12}\{E_0^*(\nabla^3 + \nabla^4)\,\Delta - hF_0^*(2\nabla^2 + \nabla^3)\,\Delta + 6h|\beta-\alpha|\,\delta_1^2\}H_0. \tag{58}$$

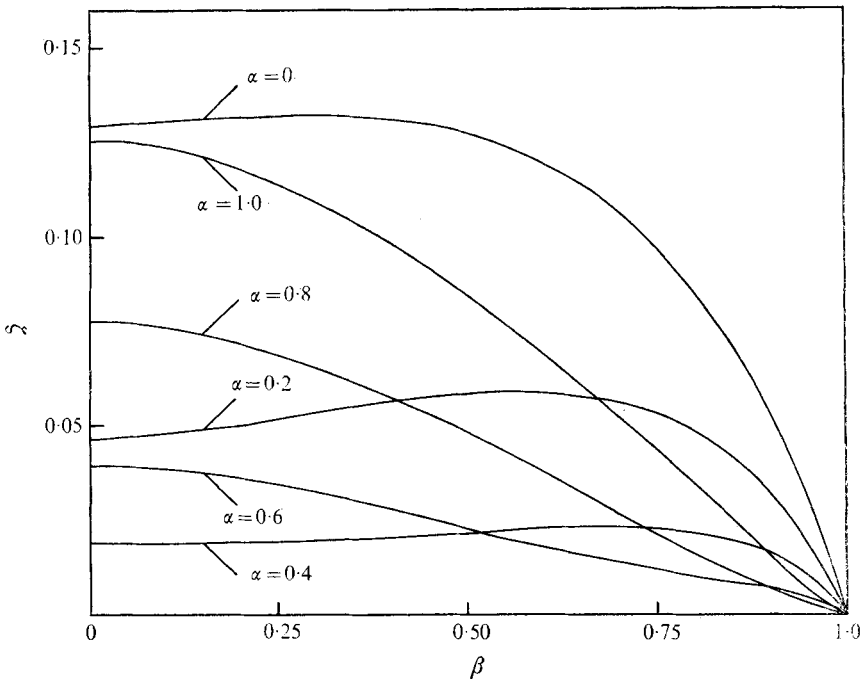

FIGURE 8. Perturbation shear stress in the I region for $P_R = 6$.

Again the corrections D_0 were evaluated from the converged solution for H obtained by neglecting D_0 and an iterative scheme analagous to the one for the correction of ζ was set up until, ultimately, overall convergence was achieved. In this manner a solution for ϕ and H was produced in the I region which is effectively accurate to $O(h^4)$ and $O(h^2)$ in the β and α directions respectively.

5.2. *Calculated results*

For all three cases considered two difference corrected solutions corresponding to grid sizes of $h = 0{\cdot}05$ and $0{\cdot}025$ were obtained in the I region as a check on the accuracy. The solutions based on the finest grid sizes in the L and M regions were used as boundary conditions at $\alpha = 0$ and $\alpha = 1$; the results presented in this section are based on the solutions for $h = 0{\cdot}025$ in the I region and are in good agreement with the solutions obtained for $h = 0{\cdot}05$. The physical parameters of the calculations, which are uniquely determined given P_R, are given in table 3 for the three cases considered. M_s is the shock Mach number.

P_R	A	B	M_s	$\mathscr{H}_1$	$\mathscr{H}_0$
2	4·6845	4·0402	1·159	−0·09656	0·1025
6	2·2750	1·5639	1·455	−0·2394	0·2903
10	1·9575	1·2177	1·608	−0·3015	0·3932

TABLE 3. Physical parameters of the solutions ($\sigma = 0{\cdot}73$, $\gamma = 1{\cdot}4$)

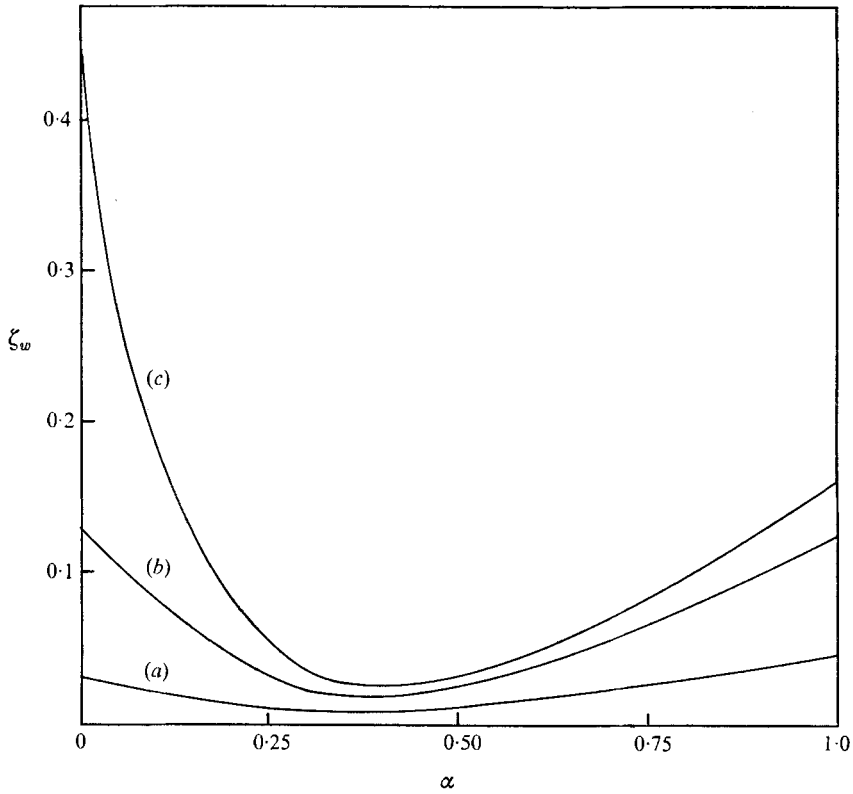

FIGURE 9. Perturbation wall shear stress ζ_w in the I region for (*a*) $P_R = 2$, (*b*) $P_R = 6$, (*c*) $P_R = 10$.

The variation of the perturbation shear stress ζ is shown in figure 8 throughout the I region for the case $P_R = 6$ and the variation of the perturbation wall shear stress ζ_w is shown in figure 9 for the three cases considered. The heat-transfer coefficient $\hat{q}_w$ is plotted in figure 10. As the I region is entered from the diaphragm, $\hat{q}_w$ is decreasing but then tends to level out and slightly increase; this effect becomes more noticeable for increasing P_R. It then decreases rapidly and eventually becomes negative. On passing through the contact surface the rate of increase lessens appreciably and eventually $\hat{q}_w$ approaches $-\infty$ at the shock wave.

The dimensionless boundary-layer thickness is plotted in figure 11 for the three cases. To illustrate the smooth transition of δ^* from the L to the I region part of the L region is included. The boundary layer thickens continuously on passing from the L to the I region reaching a maximum just past the middle. It then exhibits a tendency to decrease slightly, and subsequently thickens very rapidly near the contact surface, achieving an absolute maximum at $\alpha = 1$. The rapid thickening near the contact surface is in agreement with the solution of Ban & Kuerti (1969). This effect is caused mainly by the temperature discontinuity and thus as P_R is increased becomes more pronounced. Some evidence that this behaviour is at least qualitatively correct may be seen by examination

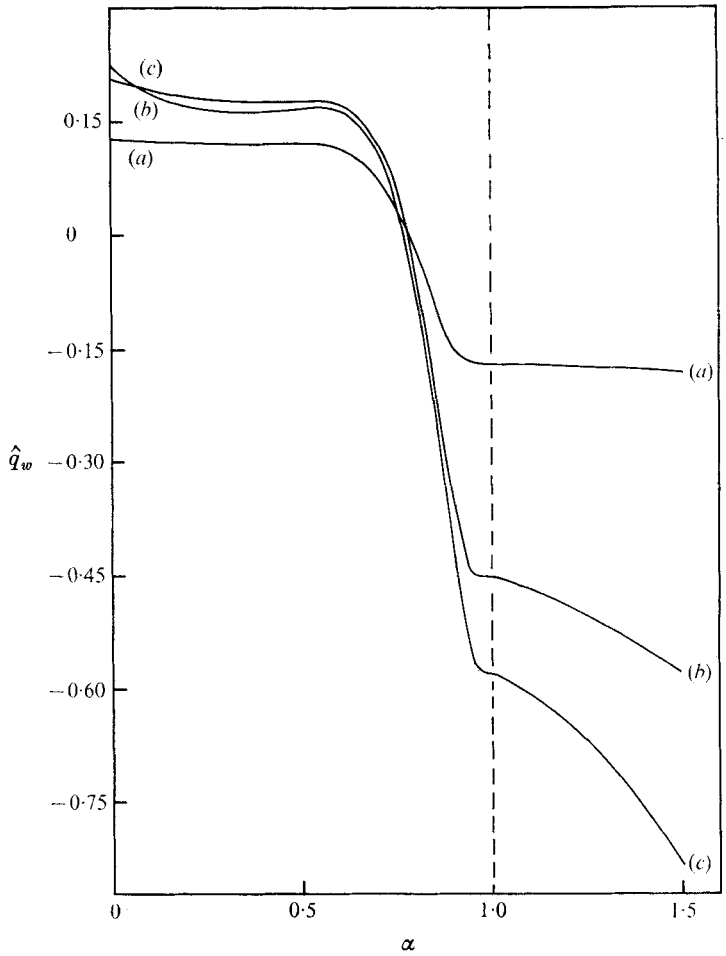

FIGURE 10. Heat-transfer coefficient in the interaction region for (a) $P_R = 2$, (b) $P_R = 6$, (c) $P_R = 10$.

of the experimental photograph obtained by Charatis & Wilkerson (1959) and reproduced by Gaydon & Hurle (1963, plate 2(a)). This photograph was for a neon–methane mixture with a shock Mach number of 6·7. The flow is turbulent in the interaction zone but a rapid thickening of the boundary layer near the contact surface is clearly evident.

The enthalpy profiles for the case $P_R = 6$ are plotted versus the dimensionless ordinate z in figure 12 in the interaction zone. Lines of constant β are plotted in figure 13 versus the dimensionless distance z from the wall, for the case $P_R = 10$. A stream function ψ may be defined by the equation $\rho u = \partial\psi/\partial y$ and a dimensionless stream function

$$\hat{\psi}(\alpha, \beta) = \frac{\psi}{U_0(\mu_w \rho_w t)^{\frac{1}{2}}} = \int_0^\beta \frac{\beta\, d\beta}{\phi}$$

may be defined. A plot of lines of constant $\hat{\psi}$, which represents lines of constant mass flux, exhibits the same general behaviour as in figure 13. Near the wall the gas passes through the contact surface almost as if unaware of the driver gas.

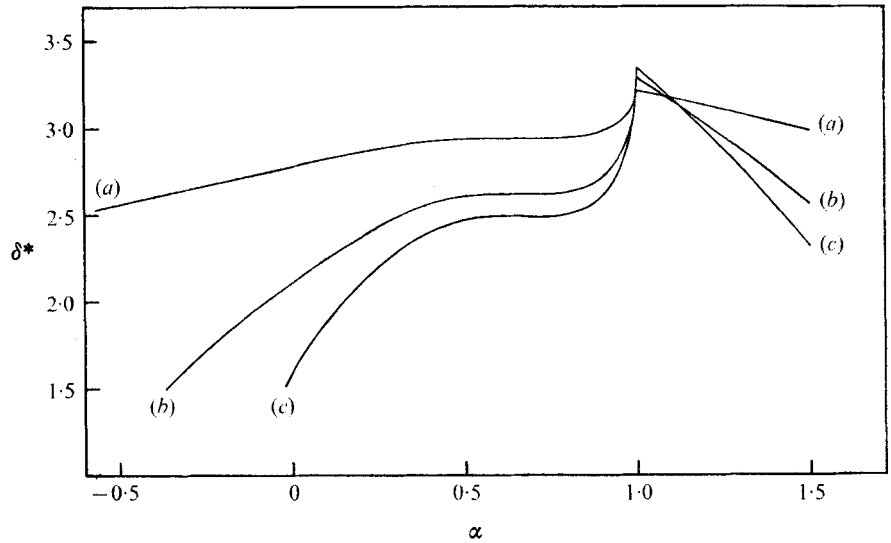

FIGURE 11. Dimensionless boundary-layer thickness δ^* in the L, I and M regions for (*a*) $P_R = 2$, (*b*) $P_R = 6$, (*c*) $P_R = 10$.

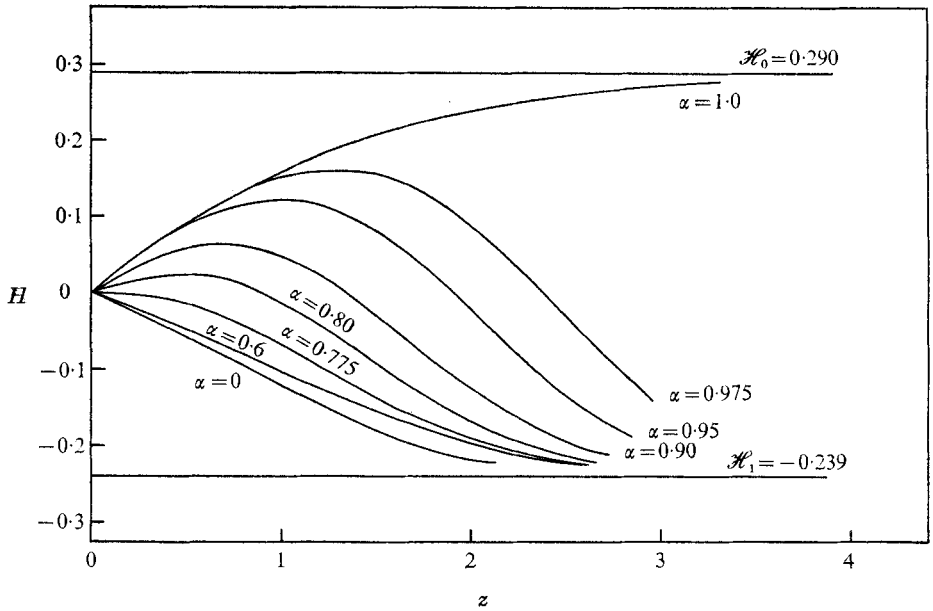

FIGURE 12. Enthalpy profiles in the interaction region for $P_R = 6$.

This is the expected result. Further away from the wall the lines of constant β degenerate from a smooth transition at the contact surface to eventually having a discontinuous slope in the upper regions of the boundary layer. Near the edge of the boundary layer the gas appears to undergo a slight compression in the right-hand half of the interaction zone. It then experiences a rapid expansion before passing through the contact surface whereupon it is continuously compressed toward the shock. The singular line where $\beta = \alpha$ is also shown in figure 13.

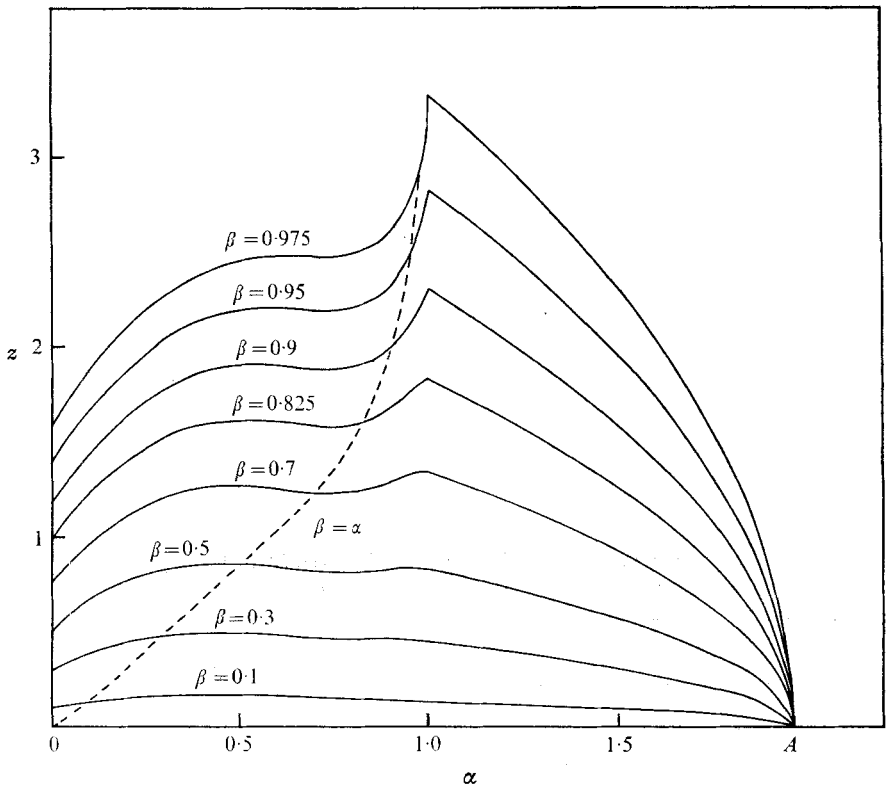

FIGURE 13. Lines of constant β in the interaction and M regions for $P_R = 10$.

6. Conclusion

In the framework of the similarity variables used, the boundary layer in a shock tube has been examined and three cases, representative of weak and medium-strength shock and expansion waves calculated. An extension of the present method could be made to the case where the expansion wave extends into the interaction zone. The interaction region would have to be divided into two regions and the forward–backward difference scheme used in each, matching the solution at the dividing boundary. If this case were considered it might be more advantageous (though not necessary) to define a new vertical co-ordinate in the fan (once the solution has been obtained at the diaphragm) in order to have a rectangular grid configuration in the overlapping E and I regions. It might be anticipated beforehand though that this may be a difficult problem since an increasing value of P_R will mean increasing gradients in the I region. For this reason, finer grid sizes might have to be used there in order to produce reliable solutions, and the increased number of mesh points alone will lead to large computing times.

Although the Crocco transformation considerably simplifies the two-dimensional boundary-layer equations, there is a well-known difficulty inherent in the transformation. This is associated with the singular behaviour of $\partial\tau/\partial u$

near $u = U_1(x,t)$ which has been described by Stewartson (1960, p. 32). The grid sizes reported in this paper were chosen after some experience and were based on a balance between the consideration of obtaining reasonable accuracy for the physical properties of the flow without an excessive amount of computation. The effect of the singularity is to preclude a high degree of accuracy, but nevertheless it is believed that a reasonable degree of accuracy can be obtained. As a representative example of this point, consider the solution for the function $M(\beta)$ as outlined in §4. Halving the grid size from $h = 0{\cdot}05$ produces a value of $M(0)$ which differs from the previous solution by about 0·1 %. Further halving of the grid successively produces a slow convergence by reducing the percentage difference successively by a factor of about 2. The difficulty, however, appears to be only one of degree and the results presented herein are believed to be reliable to at least three significant figures.

There are a number of points on which the method may be criticized. It is limited to consideration of shock tubes containing driver and driven gases that have the same thermal properties. It assumes that the flow is laminar in the tube while experimentally it is usually influenced by diaphragm-opening effects and is turbulent. It may however be argued that a first step in understanding the general problem is to compute the simplified laminar one.

Finally, the assumption of self-similar time dependence must be questioned. It is clear that the boundary-layer phenomena illustrated in figure 11 will not persist in nature for any period of time. The pressure disturbance caused by such a boundary layer will act to smooth it out and cause the contact surface to accelerate downstream. This behaviour of the contact surface has been observed experimentally (see Mirels 1971). In this sense, then, the assumption that the contact surface moves with constant speed is not strictly justified. This means that the problem is an inherently unsteady one in the similarity variables and further attempts to solve it might be based on the unsteady similarity equations whilst making some allowance for an acceleration of the contact surface. The same type of criticism applies in the region near the end of the rarefaction wave, where diffusion will act to smooth out the sharp corner in the boundary layer (see figure 6).

In conclusion, then, the results of this study must in a sense be regarded as negative although a necessary step in the ultimate solution of the shock tube problem.

The authors would like to thank Professor K. Stewartson, F.R.S. for introducing them to this subject and for several helpful suggestions, particularly the theory in the appendix, during the course of the work. They would also like to acknowledge a number of helpful discussions with Mr P. G. Williams of University College London and Prof. D. E. Abbott of Purdue University. This work was supported by a grant from the National Research Council of Canada. The results of the present paper were given at the 14th British Theoretical Mechanics Colloqium held at University College London from 10 to 13 April 1972.

Appendix

In this section, the nature of the solution in the L region is examined in the vicinity of the trailing edge of the expansion fan. Suppose that the fan terminates at $\alpha_e = -a$; then if the fan extends up to or past the diaphragm, $a \leqslant 0$ and if it ends before the diaphragm $a > 0$. Here the latter case is investigated. Consider equations (26) and (27) for the shear stress ϕ and normalized enthalpy H in similarity variables and define a dimensionless pressure $P = p/\rho_w U_0^2$. In general, at the wall ($\beta = 0$)

$$\phi\,\partial\phi/\partial\beta = \partial P/\partial\alpha, \tag{A 1}$$

and

$$\phi^2\left\{C + \frac{1}{\sigma}\frac{\partial^2 H}{\partial\beta^2}\right\} = \frac{\partial P}{\partial\alpha}\left\{C\alpha - \frac{1}{\sigma}\frac{\partial H}{\partial\beta}\right\}, \tag{A 2}$$

where $C = (\gamma-1)/B^2$. Define $\bar{x} = \alpha + a$ so that $\bar{x} = 0$ is the trailing edge of the fan. In the L region P is constant, while in the fan $P = P(\alpha)$; hence

$$\lim_{\bar{x}\to 0+} \partial P/\partial\alpha = 0 \quad \text{and} \quad \lim_{\bar{x}\to 0-} \partial P/\partial\alpha = p', \text{ say.} \tag{A 3}$$

Suppose that at $\bar{x} = 0$, $\phi = \phi_0(\beta)$ and $H = H_0(\beta)$ and for small β

$$\phi_0(\beta) = a_0 + a_1\beta + a_2\beta^2 + \ldots, \quad H_0(\beta) = b_1\beta + b_2\beta^2 + \ldots. \tag{A 4}$$

From (A 1) and (A 2)

$$a_1 = \frac{p'}{a_0}, \quad b_2 = -\frac{\sigma C}{2} - \frac{p'\sigma}{2a_0^2}\left\{Ca + \frac{b_1}{\sigma}\right\}. \tag{A 5}$$

Proceeding in the spirit of the methods given by Goldstein (1930) define

$$\xi = \bar{x}^{\frac{1}{2}}, \quad \eta = \tfrac{1}{2}\beta\bar{x}^{-\frac{1}{2}}, \tag{A 6}$$

whereupon (26) and (27) become

$$\phi^2\frac{\partial^2\phi}{\partial\eta^2} + 2\xi^2\phi = 2(2\xi\eta + a - \xi^2)\left\{\xi\frac{\partial\phi}{\partial\xi} - \eta\frac{\partial\phi}{\partial\eta}\right\}, \tag{A 7}$$

$$\phi^2\left\{4\xi^2 C + \frac{1}{\sigma}\frac{\partial^2 H}{\partial\eta^2}\right\} - d\phi\frac{\partial\phi}{\partial\eta}\frac{\partial H}{\partial\eta} = 2(2\xi\eta + a - \xi^2)\left\{\xi\frac{\partial H}{\partial\xi} - \eta\frac{\partial H}{\partial\eta}\right\}, \tag{A 8}$$

where $d = 1 - 1/\sigma$. Expansions for ϕ and H

$$\phi = f_0(\eta) + \xi f_1(\eta) + \xi^2 f_2(\eta) + \ldots, \tag{A 9}$$

$$H = \xi g_1(\eta) + \xi^2 g_2(\eta) + \ldots \tag{A 10}$$

are now assumed whence for the f_i

$$f_0^2 f_0'' + 2a\eta f_0' = 0,$$

$$f_0^2 f_1'' + 2a\eta f_1' + 2(f_0 f_0'' - a)f_1 = -4\eta^2 f_0',$$

$$f_0^2 f_2'' + 2a\eta f_2' + 2(f_0 f_0'' - 2a)f_2 = -f_1^2 f_0'' - 2f_0 f_1 f_1'' - 2f_0 + 4\eta(f_1 - \eta f_1') + 2\eta f_0'.$$

The boundary conditions for the functions f_i are that

$$\partial f_i/\partial\eta = 0 \quad \text{at} \quad \eta = 0 \quad \text{and} \quad \lim_{\eta\to\infty} f_i/\eta^i = 2^i a_i. \tag{A 11}$$

The solutions for the first three terms are

$$f_0 = a_0, \tag{A 12}$$

$$f_1 = \frac{2p'}{a^{\frac{1}{2}}}\left\{z\,\mathrm{erf}\,z + \frac{e^{-z^2}}{\pi^{\frac{1}{2}}}\right\}, \tag{A 13}$$

$$f_2 = A_2(2z^2+1) + B_2\left\{(2z^2+1)\,(\mathrm{erf}\,z - 1) + \frac{2z\,e^{-z^2}}{\pi^{\frac{1}{2}}}\right\}$$
$$+ \frac{a_0}{2a} - \frac{p'a_0 z\,e^{-z^2}}{\pi^{\frac{1}{2}}a^2} - \frac{p'^2}{a_0 a\pi^{\frac{1}{2}}}\{\pi^{\frac{1}{2}}(2z^2+1)\,(\mathrm{erf}\,z)^2 + 2z\,e^{-z^2}\,\mathrm{erf}\,z\}, \tag{A 14}$$

where $z = a^{\frac{1}{2}}\eta/a_0$ and A_2 and B_2 are constants such that

$$A_2 = (1/aa_0)\{2a_2a_0^3 + p'^2\}, \quad B_2 = p'a_0/4a^2. \tag{A 15}$$

The equation for the first two functions in the expansion (A 10) are

$$(f_0^2/\sigma)\,g_1'' + 2a\eta g_1' - 2ag_1 = 0,$$
$$(f_0^2/\sigma)\,g_2'' + 2a\eta g_2' - 4ag_2 = -4Cf_0^2 + df_0f_1'g_1' - (2/\sigma)f_0f_1g_1'' + 4\eta(g_1 - \eta g_1'),$$

and the solutions of these equations satisfying the boundary conditions

$$g_i(0) = 0 \quad \text{and} \quad \lim_{\eta\to\infty} g_i/\eta^i = 2^ib_i$$

are

$$g_1 = 2b_1\eta,$$
$$g_2 = -\frac{2a_0^2C}{a}z^{*2} - p'C\left\{(2z^{*2}+1)\,\mathrm{erf}\,z^* + \frac{2z^*\,e^{-z^{*2}}}{\pi^{\frac{1}{2}}}\right\} - \frac{p'b_1}{a}\left\{(2z^2+1)\,\mathrm{erf}\,z + \frac{2z\,e^{-z^2}}{\pi^{\frac{1}{2}}}\right\},$$

where $z^* = (a\sigma)^{\frac{1}{2}}\eta/a_0$.

The solution given by (A 9) and (A 10) is valid in an inner region near $\beta = 0$, where $\beta \sim \bar{x}^{\frac{1}{2}}$. The asymptotic form of the expansions (A 9) and (A 10) as $\eta \to \infty$ is

$$\phi \to a_0 + 2a_1\xi\eta + \xi^2\{4a_2\eta^2 + (4a_2a_0^2 + a_0)/2a\} + O(\xi^3), \tag{A 16}$$

$$H \to 2b_1\xi\eta + \xi^2[4b_2\eta^2 + (1/a)\{2b_2a_0^2/\sigma - p'b_1d + a_0^2C\}] + O(\xi^3), \tag{A 17}$$

and this suggests that in the outer region, where $\beta \sim 1$, ϕ and H are of the form

$$\left.\begin{aligned}\phi &= \phi_0(\beta) + \bar{x}\phi_1(\beta) + O(\bar{x}^2),\\ H &= H_0(\beta) + \bar{x}H_1(\beta) + O(\bar{x}^2).\end{aligned}\right\} \tag{A 18}$$

Substitution in (26) and (27) implies that

$$\phi_1(\beta) = \frac{1}{(\beta+a)}\{\phi_0^2\phi_0'' + \tfrac{1}{2}\phi_0\},$$
$$H_1(\beta) = \frac{1}{(\beta+a)}\left\{\phi_0^2\left(C + \frac{1}{\sigma}H_0''\right) - d\phi_0\phi_0'H_0'\right\},$$

and it is easily verified that the outer solution (A 18) as $\beta \to 0$ matches the inner solution (A 9) and (A 10) as $\eta \to \infty$.

The inner solution (A 9) indicates that on the wall

$$\phi(\alpha, 0) = a_0 + (2p'/(a\pi)^{\frac{1}{2}})\,\bar{x}^{\frac{1}{2}} + O(\bar{x}). \tag{A 19}$$

$\bar{x}$	$\phi_w\|_N$	$\phi_w\|_c$	$\hat{q}_w\|_N$	$\hat{q}_w\|_c$
0	1·4874	1·4874	0·3431	0·3431
$4{\cdot}69\times10^{-4}$	1·4301	1·4268	0·3364	0·3366
$9{\cdot}38\times10^{-4}$	1·4075	1·4018	0·3335	0·3338
$1{\cdot}41\times10^{-3}$	1·3907	1·3825	0·3313	0·3318
$1{\cdot}86\times10^{-3}$	1·3774	1·3668	0·3295	0·3301
$2{\cdot}33\times10^{-3}$	1·3654	1·3525	0·3279	0·3285
$2{\cdot}80\times10^{-3}$	1·3548	1·3395	0·3264	0·3271

TABLE 4. Comparison of numerical and inner solution for $P_R = 6$

The reason for the numerical difficulty at the end of the fan is now clear. Recalling that the numerical procedure (32) was not applied on the wall itself, nevertheless the α derivatives of ϕ, upon which the truncation error in (32) depends, will be large near the wall at the end of the fan; this requires the use of small grid sizes in this region. Noting that

$$p' = -\frac{2B}{\gamma+1}\left\{1-\frac{\gamma-1}{2B}\right\}^{-1},$$

a comparison of the values of ϕ on the wall obtained from the numerical solution for $P_R = 6$ (denoted by $\phi_w|_N$) and that obtained from the first two terms of (A 19) (denoted by $\phi_w|_c$) is given in table 4 for various values of $\bar{x}$. One further comparison is possible. The inner solution (A 9) and (A 10) gives the following expression for the heat-transfer coefficient $\hat{q}_w$:

$$\hat{q}_w = \hat{q}_w|_{\bar{x}=0} + \frac{2p'}{B^2}\left(\frac{a}{\sigma\pi}\right)^{\frac{1}{2}}\left\{1-\frac{\gamma-1}{2B}\right\}^{\gamma/(\gamma-1)}\bar{x}^{\frac{1}{2}} + O(\bar{x}), \tag{A 20}$$

and this quantity is compared with the numerical solution $\hat{q}_w|_N$ for $P_R = 6$ in table 4. There $\hat{q}_w|_c$ represents the first two terms of (A 20).

Finally the nature of the boundary-layer thickness δ^* (defined in §3.3) may be examined near the end of the fan. Splitting the integral for δ^* into two parts gives

$$\delta^*(\bar{x}) = 2\xi\int_0^{\eta_1}\frac{H+1}{\phi}\,d\eta + \int_{2\eta_1\bar{x}^{\frac{1}{2}}}^{0\cdot975}\frac{H+1}{\phi}\,d\beta, \tag{A 21}$$

where $\bar{x}$ is small and η_1 is some large value of η. In the inner region, ϕ and H are written as

$$\left.\begin{aligned}\phi &= \phi_0(\beta)+\xi\bar{f}_1+\xi^2\bar{f}_2+O(\xi^3),\\ H &= H_0(\beta)+\xi^2\bar{g}_2+O(\xi^3),\end{aligned}\right\} \tag{A 22}$$

where

$$\bar{f}_1 = f_1(\eta)-2a_1\eta,\quad \bar{f}_2 = f_2(\eta)-4a_2\eta^2,\quad \bar{g}_2 = g_2(\eta)-4b_2\eta^2.$$

Substitution of the expressions (A 22) into the first integral in (A 21) and the outer solution (A 18) into the second integral leads to

$$\delta^*(\bar{x}) = \int_0^{0\cdot975}\frac{H_0+1}{\phi_0}\,d\beta - \frac{2\xi^2}{a_0^2}\int_0^{\eta_1}\bar{f}_1(\eta)\,d\eta + \bar{x}\int_{2\eta_1\bar{x}^{\frac{1}{2}}}^{0\cdot975}\left\{\frac{H_1\phi_0-\phi_1(H_0+1)}{\phi_0^2}\right\}d\beta + O(\bar{x}^{\frac{3}{2}}).$$

For $\bar{x}$ small, the lower limit in the third integral may be replaced by 0 and the upper limit in the second by ∞. Hence

$$\delta^*(\bar{x}) = \delta^*(0) - \frac{p'\bar{x}}{aa_0} + \bar{x}\int_0^{0\cdot975} \frac{(H_1\phi_0 - \phi_1(H_0+1))}{\phi_0^2}\,d\beta + O(\bar{x}^{\frac{3}{2}}).$$

Here $\delta^*(0)$ is the boundary-layer thickness at the end of the fan. Since p' is negative, removal of the pressure gradient causes an added increase in δ^* at the end of the fan and with increasing P_R this will become more pronounced (see figure 6).

REFERENCES

BAN, S. D. & KUERTI, G. 1969 *J. Fluid Mech.* **38**, 109.

BECKER, E. 1962 *Z. Flugwiss.* **10**, 4/5, 138.

BLASIUS, H. 1908 *Z. Math. Phys.* **56**, 1.

CHAPMAN, D. R. & RUBESIN, M. W. 1949 *J. Aero. Sci.* **16**, 547.

CHARATIS, G. & WILKERSON, T. D. 1959 *Phys. Fluids*, **2**, 578.

COHEN, N. B. 1957 *N.A.C.A. Tech. Note*, no. 3943.

DENNIS, S. C. R. 1972 *J. Inst. Math. Applics.* **10**, 105.

DENNIS, S. C. R. & WALKER, J. D. A. 1972 *Phys. Fluids*, **15**, 517.

FOX, L. 1957 *The Numerical Solution of Two-Point Boundary Value Problems.* Oxford University Press.

GAYDON, A. G. & HURLE, I. R. 1963 *The Shock Tube in High Temperature Chemical Physics.* New York: Reinhold.

GOLDSTEIN, S. 1930 *Proc. Camb. Phil. Soc.* **26**, 1.

GREENSPAN, D. 1968 In *Lectures on the Numerical Solution of Linear, Singular and Non-linear Differential Equations*, chap. 10. Prentice Hall.

HALL, M. G. 1969 *Proc. Roy. Soc.* A **310**, 401.

LAM, S. H. & CROCCO, L. 1958 *Princeton Rep.* no. 428. (See also *AFOSR Tech. Note*, no. 58–581.)

MIRELS, H. 1955 *N.A.C.A. Tech. Note*, no. 3401.

MIRELS, H. 1956 *N.A.CA. Tech. Note*, no. 3712.

MIRELS, H. 1971 In *Shock Tube Research, Proc. 8th International Shock Tube Symp. Imperial College, London*, pt. 6. Chapman & Hall.

RAYLEIGH, LORD 1911 *Phil. Mag.* **21**, 697.

ROSSER, J. B. 1967 *Mathematics Research Centre, University of Wisconsin, Tech. Summ. Rep.* no. 797.

SHAPIRO, A. H. 1960 *The Dynamics and Thermodynamics of Compressible Fluid Flow.* New York: Ronald Press.

SPALDING, D. B. 1967 *Numerical Methods for Viscous Flows, AGARD Conf. Proc.* no. 60.

STEWARSON, K. 1951 *Quart. J. Mech. Appl. Math.* **4**, 182.

STEWARTSON, K. 1960 *Adv. Appl. Mech.* **6**, 1.

STEWARTSON, K. 1964 *The Theory of Laminar Boundary Layers in Compressible Fluids.* Oxford University Press.

STEWARTSON, K. 1972 *Quart. J. Mech. Appl. Math.* to appear.

VARGA, R. S. 1962 *Matrix Iterative Analysis.* Prentice-Hall.

WALKER, J. D. A. 1971 Ph.D. thesis (appendix V), University of Western Ontario, London, Canada.